Spring 3-29-2018

INVESTIGATION OF ANION AND CATION EXCHANGE MEMBRANES FOR ENHANCING DESALINATION AND POWER GENERATION IN A MICROBIAL DESALINATION CELL

Francisco Lopez Moruno
University of New Mexico

Francisco Lopez Moruno
Candidate

Civil Engineering
Department

This thesis is approved, and it is acceptable in quality and form for publication:

Approved by the Thesis Committee:

Dr. José Manuel Cerrato, Chairperson

Dr. Plamen Atanassov

Dr. Andrew Schuler

Dr. Carlo Santoro

INVESTIGATION OF ANION AND CATION EXCHANGE MEMBRANES FOR ENHANCING DESALINATION AND POWER GENERATION IN A MICROBIAL DESALINATION CELL

by

FRANCISCO LOPEZ MORUNO

B.S., CIVIL ENGINEERING, UNIVERSITY OF GRANADA,
SPAIN, 2016

THESIS

Submitted in Partial Fulfillment of the
Requirements for the Degree of

Master of Science in Civil Engineering

The University of New Mexico
Albuquerque, New Mexico

May, 2018

ACKNOWLEDGMENTS

I would like to thank my advisors Dr. Cerrato and Dr. Atanassov for their mentorship and fully support in this graduate program. Dr. Rages, from LSU, for his membrane characterization and fully collaboration. I also would like to thank Dr. Schuler for agreeing to serve on my committee. Finally, I want to express my gratitude to Dr. Santoro for his guidance, who without his help and knowledge this research would have not been possible.

Preface

The following papers have been published base on the work of this thesis.

1. Moruno, F. L., Rubio, J. E., Santoro, C., Atanassov, P., Cerrato, J. M., & Arges, C. G. (2018). Investigation of patterned and non-patterned poly (2, 6-dimethyl 1, 4-phenylene) oxide based anion exchange membranes for enhanced desalination and power generation in a microbial desalination cell. Solid State Ionics, 314, 141-148.
2. Moruno, F. L., Rubio, J. E., Atanassov, P., Cerrato, J. M., Arges, C. G., & Santoro, C. (2018). Microbial desalination cell with sulfonated sodium polyether ether ketone as cation exchange membranes for enhancing power generation and desalination. Bioelectrochemistry, 121, 176-184.

INVESTIGATION OF ANION AND CATION EXCHANGE MEMBRANES FOR ENHANCING DESALINATION AND POWER GENERATION IN A MICROBIAL DESALINATION CELL

by

FRANCISCO LOPEZ MORUNO

B.S., CIVIL ENGINEERING, UNIVERSITY OF GRANADA,
SPAIN, 2016
M.S., CIVIL ENGINEERING, UNIVERSITY OF NEW MEXICO,
USA, 2018

ABSTRACT

Microbial desalination cell (MDC) is a bioelectrochemical system capable of oxidizing organics, generating electricity and reducing the salinity content into the desalination chamber. As it is designed, anion and cation exchange membranes play an important role on the selective removal of ions from the desalination chamber. In the first part of this study, quaternary ammonium poly(2,6-dimethyl 1,4-phenylene oxide) (QAPPO) anion exchange membranes (AEMs) with topographically patterned surfaces were assessed in a microbial desalination cell (MDC) system. The MDC results with these QAPPO AEMs were benchmarked against a commercially available AEM. The

MDC with the non-patterned QAPPO AEM (Q1) displayed the best desalination rate (a reduction of salinity by 53±3 %) and power generation (189±5 mW m^{-2}) when compared against the commercially available AEM and the patterned AEMs. The enhanced performance with the Q1 AEM was attributed to its higher ionic conductivity and smaller thickness leading to a reduced area specific resistance. The non-patterned QAPPO AEM displayed better performance over the patterned QAPPO AEMs. In the second part of this study, sulfonated sodium (Na^+) poly(ether ketone) (SPEEK) cation exchange membranes (CEMs) were tested in combination with quaternary ammonium chloride poly(2,6-dimethyl 1,4-phenylene oxide) (QAPPO) anion exchange membrane (AEM). Non-patterned and patterned (with increased, lateral different topographical features) CEMs were investigated and assessed in this work. The results were also contrasted against a commercially available CEM. The results for QAPPO/SPEEK displayed a higher desalination rate and power generation than commercial membranes, with a maximum of 78.6±2 % in salinity reduction and 235±7 mW m^{-2} in power generation for the MDCs with a non-patterned (i.e., flat) CEM. Desalination rate and power generation achieved were higher with synthesized SPEEK membranes when compared with an available commercial CEM. It is important to note that Real Pacific Ocean seawater and activated sludge were used into the desalination chamber and anode chamber respectively for the MDC – which mimicked realistic conditions. An optimized combination of these types of membranes substantially improves the performances of this bioelectrochemical system.

TABLE OF CONTENTS

List of Figures

List of Tables

Chapter 1. Introduction

1.1. Scope of the Thesis

The objective of this study is to investigate the electrochemical performance of a MDC in terms of power density and desalination rate utilizing different anion exchange membranes and cation exchange membranes. AEMs and CEMs with non-patterned and patterned topographical features were tested. The MDC cell was examined using three different solutions in each chamber: i) activated sludge; ii) Pacific Ocean seawater; and iii) 10 mM potassium phosphate buffer (K-PB). Operating parameters, such as pH and solution conductivity, were monitored during the experiments to estimate the desalination rate. The operating conditions and desired outputs, power density and desalination rate, of the MDC with different laboratory membranes were benchmarked against commercial membranes.

1.2. Outline of the Thesis

This thesis includes six chapters. Chapter 1. Introduction exposes water concerns, currently water technologies used and review focuses on specific microbial desalination technology. Chapter 2. Displays materials and methods used, as well as operation conditions. Chapter 3. First part, shows results and discussion using laboratory made AEMs in combination with commercial CEM. Chapter 3. Second part, shows improvements obtained using combination of non-patterned laboratory AEM with different novel laboratory CEMs. Chapter 4. Comprises general conclusions and Chapter 5. Outlook for both investigations. Finally, in Chapter 6. We acknowledge fund contributors that did possible this research.

1.3. Motivation and microbial desalination cell technology

At the 1800´s century, Luigi Galvani started the first experiments in the field of electrochemical and bio-electrochemical, but after this not much research focused on the possible practical applications using electrochemical properties. Around 2005, we can see how the research papers about Bio-electrochemical Systems (BES) grew up considerably, specially, due to the fact of trying to look for new ways of sustainable designs for water treatment, produce electricity, desalination, etc. Becoming the microbial fuel cell systems (MFC) (**Figure 1.**) an important field of research with connections to inter-disciplinary fields. MFCs are considered by the research community as interesting way to possible self-sustainable production of electricity and water-treatment. Initially, it was introduced the idea of microbial electrolysis cell (MEC), with the main purpose of producing hydrogen. This device needs electricity input from an external source for electricity to produce hydrogen at the cathode, which is becoming in an important gas for future based hydrogen economy.

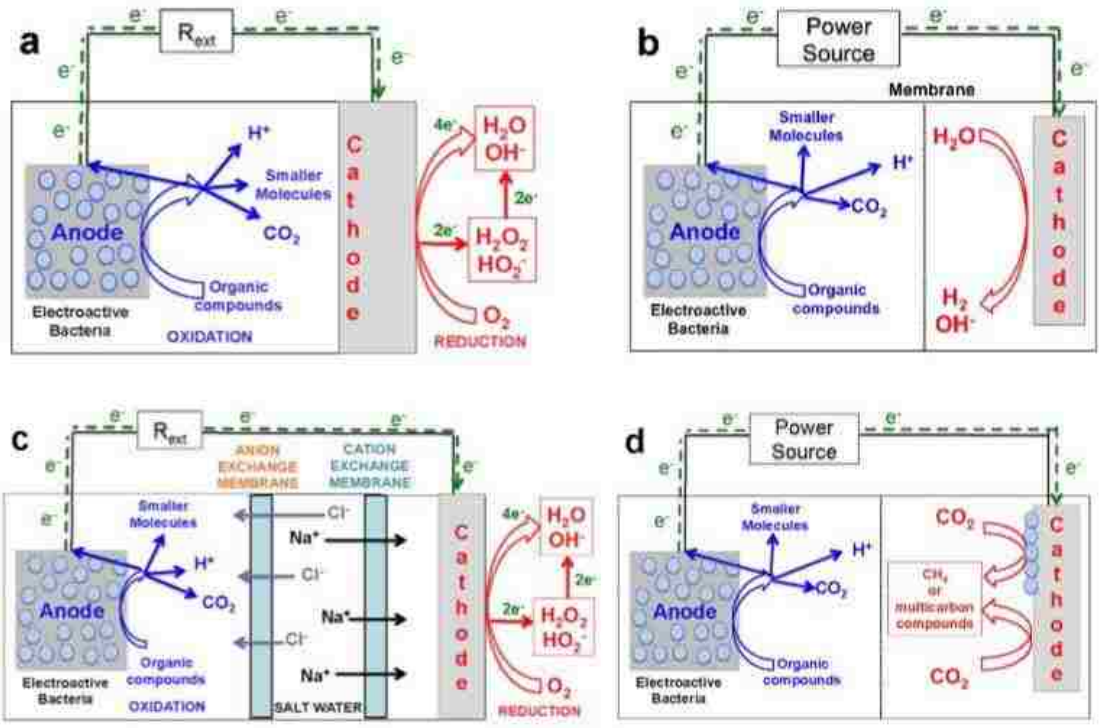

Figure 1. Schematic of a microbial fuel cell (a), microbial electrolysis (b), microbial desalination cell (c) and general microbial electrosynthesis cell (d).
(Picture from C.Santoro et al. /Journal of Power Sources 356 (2017) 225-244)

One alternative desalination technology under consideration since 2009 is a microbial desalination cell (MDC), a type of bio-electrochemical cell [14-17]. MDC is a technology with trigenerative aspects such as wastewater treatment, electricity generation and water desalination. A MDC (**Figure 2.c.**) is a galvanic, self-sustainable bioelectrochemical system (BES), in which electroactive bacteria are able to convert organics and pollutants at the anode into electrical energy through the biological and electrochemical reactions [18]. Therefore, at the anode there is an oxidation process, in this case due to the feed with acetate, the reaction is $CH_3CO_2Na + 2H_2O \rightarrow 2CO_2 + 7H^+ + 8e^- + Na^+$, decreasing pH at the anode due to H^+ production. At the cathode, oxygen is electrochemically reduced to complete the circuit [14-18], oxygen is used as electron acceptor which in basic media with carbonaceous base cathode, there is $2e^-$ transfer reaction and production OH^-, increasing pH at the cathode ($H_2O + O_2 + 2e^- \rightarrow H_2O^- +$

OH^-). This system has a central chamber separated from the other two chambers (anode and cathode chamber) by an anion and cation exchange membrane. The selective membranes allow the transfer of ions from the salty water (mainly Na+ and Cl-) to the other chambers. A unique feature of the MDC is that it can reduce the salinity content in the central chamber, while co-currently producing electrical energy through electrochemical oxidation of organics and pollutants [14-18].

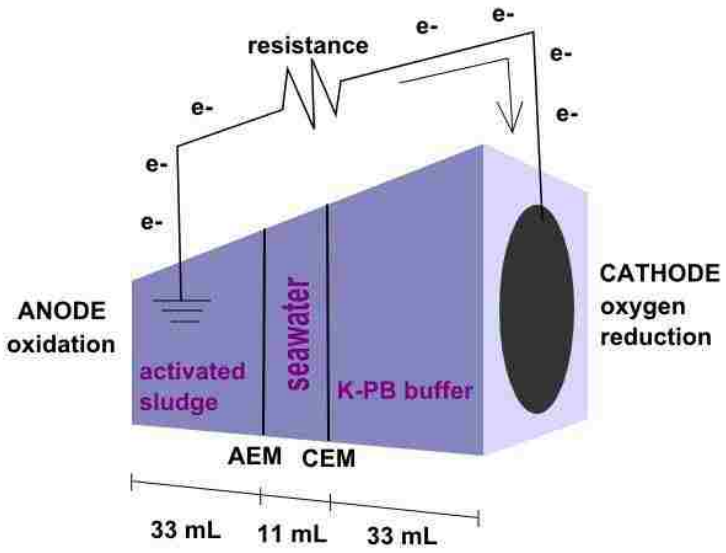

Figure 2. Schematic of microbial desalination cell set up used for this study.

Despite the innovative aspects regards to MDCs, there are existing issues with this technology that require improvement. The different, and diverse, elements in MDC can vary significantly altering the desired objectives of the technology (e.g., power output and desalination amount). In the case of MFCs systems, different configurations have been developed from lab-scales to higher volumes with examples of 20 L [19-20], 45 L [21], 72 L [22], 250 L [23] and up to a maximum of 1000 L [24]. However, MDC systems have not been scaled beyond 100 L pilot plant systems [25], but the scaled MDC revealed that the technology requires significant resolution to a plethora of

problems to make it commercially lucrative. In particular, the principal problems related with MDCs are: low electrochemical performances, poor chemical oxygen demand (COD) degradation, and unsatisfactory desalination rates [26-33]. Several investigations have aimed to improve the MDC system by optimizing the design of elements as electrode materials. The ultimate goal is to enhance energy recovery and extract higher desalination rates [26-33]. Cathodic reactions for the MDC has been investigated with either a potassium ferricyanide or oxygen reductant species. Oxygen was the more appropriate species as it is: i) its natural availability; ii) low cost; and iii) has a high reduction potential [34]. Other different approaches were pursued to enhance the system as for example the utilization of biocathodes, bipolar membranes, capacitive features, or recirculation [15-16]. In parallel, low content of easily degradable chemical oxygen demand (COD) present in the wastewater that is used as fuel from the microorganisms at the anode, negatively affect the anodic electro-kinetics [15-16]. Greater improvements related to anode and cathode, as well as the membranes, are important priorities to enhance the sluggish electrochemical performances.

Initial study of microbial desalination cell technology was investigated by X. Cao in 2009 [14], using AEM (DF120, Tianwei Membrane) and CEM (Ultrex CMI-7000, Membranes International) obtained good results. Investigations conducted by other research groups have also used mostly commercially available membrane from Membranes International INC. New Jersey, USA (AEM AMI-7000 and CEM CMI-7000) [27, 31, 35]. However, the effect of using different AEMs and CEMs to improve the performances and the desalination rate has been overlooked. This serves as a motivation for the investigation of novel AEMs and CEMs in this study which could be a feasible way to further enhance the performances of MDCs, especially in terms on

power generation and reduction in salt content. For those reasons, future research in bioelectrochemical systems (BESs) in wastewater treatment should consider scaling up as a critical issue. Ion exchanges membranes strongly impact the electrochemical performance of MDC, because the membranes makeup a significant resistance contribution (i.e., the ohmic overpotential or ohmic loses) in the assembled cell affecting the overall power generation and desalination rate. Mitigating the membrane resistance can be achieved by adjusting its thickness, selectivity and ionic conductivity.

Chapter 2. Materials and methods

2.1. Electrodes used in microbial desalination cells

As MDC schematic is shown in **Figure 2.,** anode and cathode electrodes were inserted in the anode chamber and cathode chamber respectively. The anode electrode was a carbon brush with a cylindrical shape, a diameter of 3 cm and height of 3 cm. Carbon brushes were built with carbon fibers wrapped on a titanium core (Millirose, USA). Before their use, each anode electrode was kept in a separate microbial fuel cell and the anode was already colonized with electroactive bacteria and well working before using the anodes for the MDCs experimentation [36-37]. The cathode electrode was designed in air-breathing configuration in order to have a three phase interface (TPI) and therefore be able to utilize oxygen in gas phase. New unused cathodes were fabricated and used during each cycle for consistency. The cathodes were based on activated carbon (AC), carbon black (CB) and polytetrafluoroethylene (PTFE) blended in a blender with a mixing ratio in weight of 8:1:2 of AC/CB/PTFE. The black powder obtained was inserted into a pellet die and then pressed over a stainless-steel mesh used as current collector through a hydraulic press at 2 mT for 5 min. The loading of AC/CB/PTFE for each cathode was 40 mg cm^{-2} and 7 cm^2 of circular geometric area was exposed to the electrolyte [36-37]. Equal area of the cathode from the other side was exposed to the atmosphere.

2.2. Set up and operating conditions

The system used for this study consisted was an MDC having three separated chambers (anodic, desalination and cathodic chamber), an anode electrode (immersed into the anodic chamber), an air-breathing cathode, and two exchange membranes separating the three chambers. This setup is illustrated in **Figure 3.** Anodic and cathodic chambers had a volume of 33 mL, instead the desalination chamber had a volume of 11 mL [38-39]. The anode chamber was filled with a 33 mL solution of activated sludge taken from Albuquerque Southeast Water Reclamation Facility. The initial pH of the sludge was 7.8 and it had an initial conductivity of 2.1 mS cm^{-1}. The solution was fully replenished for every cycle. The central chamber of the system, named desalination chamber, was filled with 11 mL of real seawater (51.4 mS cm^{-1}) collected from the Pacific Ocean in Solana Beach –CA- USA. An anion exchange membrane (AEM) separated the anode chamber from the desalination chamber. The cation exchange membrane (CEM) separated the cathode chamber from the desalination chamber. The data recorded at the study was based on 3 days cycles for each cell, doing a total of 3 cycles for each combination of membranes (triplicate results). MDCs experiments were run always using the same operating conditions.

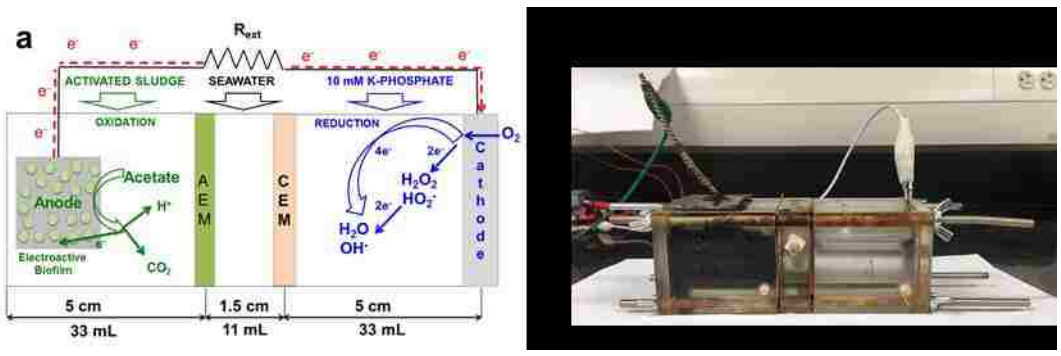

Figure 3. Microbial desalination cell (MDC) setup used for this study (a) MDC schematic; and (b) picture of operating MDC.

2.3. Membrane materials: fabrication and characterization

2.3.1. QAPPO Anion exchange membranes

Anion and cation exchange membrane were used to physically separate the desalination chamber, positioned between the anode and the cathode chamber respectively. The cation exchange membrane (CEM) utilized during this experiment was a commercial cation exchange membrane, CEM CMI-7000S, 0.45 mm, (from Membranes International INC., NJ, USA). In case of AEM, all other chemicals used to make PPO were sourced from VWR except 2,2′-Azobis(2-methylpropionitrile) (AIBN – free radical initiator – 99%, recrystallized), which was attained from Sigma-Aldrich.

AEMs composed of poly(2,6-dimethyl 1,4-phenylene oxide) (PPO) with quaternary benzyl trimethylammonium chloride moieties were synthesized as reported in the literature [40]. The synthesis procedure is briefly summarized here: PPO was dissolved in chlorobenzene (8wt%) at room temperature. The dissolved polymer was transferred to a round bottom flask with an egg-shaped stir bar. N-bromosuccimide (NBS) was added (0.7:1 molar ratio to PPO repeat unit). The reaction solution was heated to 130 °C. The free radical initiator AIBN was added (2wt% to the amount of PPO dissolved). After reacting the solution for 18 hours, the reaction solution was cooled to room temperature and was precipitated in methanol (5:1 volume ratio). The collected polymer was then dissolved in chloroform and precipitated in the methanol (5:1 volume ratio) to remove impurities. Then, brominated PPO (BrPPO) was dissolved in n-methyl-2-pyrrolidone to make a 5wt% solution. 40wt% of trimethylamine water was added in limiting reagent (0.5 trimethylamine to bromomethyl group). Note: Trimethylamine was added in limiting reagent to prevent excess swelling of the QAPPO AEM in a fully flooded cell. The unreacted bromomethyl groups self-crosslinked to reinforce the membrane's mechanical properties [41]. The reaction was

stirred at room temperature for 48 hours and then drop casted onto substrates to prepare non-patterned and patterned AEMs. The AEMs were then removed from the substrates by immersing in deionized water and peeling the membranes off the substrate. 50 μm thick QAPPO AEMs were attained. The QAPPO AEMs were ion-exchanged from the bromide counterion to the chloride counterion by immersion in 1 M sodium chloride (NaCl) overnight followed by immersion and excess rinse with deionized water to remove residual salt ions.

The QAPPO AEMs with different periodic, topographical patterns were prepared by drop casting the dissolved QAPPO solution in NMP on to micropatterned poly(dimethyl siloxane) (PDMS) molds that were prepared through conventional soft lithography. The different lateral feature sizes of the patterned QAPPO AEMs were: 20 (Q2), 33 (Q3), 40 (Q4), and 80 (Q5) μm). The non-patterned QAPPO AEM (Q1) was drop casted onto a flat glass substrate.

The conversion of the base polymer, PPO, to BrPPO was confirmed via 1H NMR spectroscopy using deuterated chloroform (CDCl3) solvent that contained tetramethylsilane (TMS) as an internal standard. The NMR spectrometer was 400 MHz Bruker instrument. The amount of bromine added to the PPO backbone was determined by integrating the 1H NMR spectra according to the literature [40]. The ionic conductivity of the non-patterned QAPPO AEMs was determined by electrochemical impedance spectroscopy (EIS) using a 4-point platinum conductivity probe. EIS, in galvanostat mode, was performed with a 2 mA amplitude in the frequency range of 100,000 Hz to 0.1 Hz. The in-plane resistance was determined from the Bode plot, where the resistance value had a phase angle value of zero, and was used in equation 1 (eq. 1) to determine the in-plane ionic conductivity (σ).

$$\sigma = \frac{L}{R \times t \times w} \quad \text{(eq.1)}$$

where σ was the in-plane conductivity, R was the in-plane membrane resistance, t was the membrane thickness (fully hydrated membrane) and w was the membrane width (fully hydrated membrane).

As check control and comparison for this study, a AMI-7001S AEM (from Membranes International INC. NJ, USA) was also assessed in MDC cell. The through plane resistance for this membrane and thickness, as stated by the manufacturer, is: < 40 ohm-cm^2 and 450 μm [42].

2.3.2. SPEEK Cation exchange membranes

SPEEK CEMs were synthesized as reported in the literature [43]. Poly(arylene ether ether ketone) (PEEK) was dissolved in concentrated sulfuric acid (10 wt% in 98% pure sulfuric acid solution) and was mixed for 72 hours at room temperature. The polymer was precipitated in an ice-cold bath and repeatedly washed and filtered until the pH of the washing water was 7. A 5 wt% SPEEK solution in n-methyl pyrrolidine (NMP) was prepared and the solution was drop casted on to 15 cm x 15 cm glass plate placed on a leveled surface in an oven. The oven temperature was then set to 70 °C and the solvent was evaporated over 18 hours. The membrane on the glass plate was immersed in deionized water to remove it. Note: This is the flat SPEEK sample (S1). The resulting thickness of the membrane, after drying, was approximately 30 μm. The SPEEK CEM was ion-exchanged to the sodium ion form by immersing the membrane in 1 M sodium hydroxide (NaOH) solution for 18 hours followed by excessive rinsing and immersion in deionized water to remove excess salt.

The conversion of the base polymer, PEEK, to SPEEK was confirmed via 1H NMR spectroscopy using deuterated dimethyl sulfoxide (d-DMSO) solvent that contained tetramethylsilane (TMS) as an internal standard. The NMR spectrometer was

400 MHz Bruker instrument. The amount of sulfonate groups per repeat unit (the degree of functionalization (DF)) was determined by integrating the 1H NMR spectra (see equation 1). **Figure 4.a** gives the chemical reaction for converting PEEK into SPEEK and **Figure 4.b** is the 1H NMR spectrum.

$$DF = \frac{Area_a}{Area_b} \qquad <1>$$

The SPEEK CEMs with different periodic, topographical patterns were prepared by drop casting the dissolved SPEEK solution in NMP on to micropatterned poly(dimethyl siloxane) (PDMS) molds that were prepared through conventional soft lithography as described in our previous report [44]. The different lateral feature sizes of the patterned SPEEK CEMs were: 20 (S2), 33 (S3), 40 (S4), and 80 (S5) μm). **Figure 5.a** depicts the general scheme to create SPEEK CEMs with topographical patterns. The micropatterned SPEEK membrane surfaces were imaged with a Nikon OPTIPHOT-88 Optical Microscope. **Figure 5.b** shows optical micrographs of two of the micropatterned SPEEK CEMs with different topographical lateral feature sizes.

The in-plane ionic conductivity of the SPEEK CEMs was determined by electrochemical impedance spectroscopy (EIS) using a 4-point platinum conductivity probe in deionized water and 0.5 g L^{-1} sodium chloride (NaCl). EIS, in galvanostat mode, was performed with a 2 mA amplitude in the frequency range of 100,000 Hz to 0.1 Hz. The in-plane resistance was determined from the Bode plot, where the resistance value had a phase angle value of zero, and was used in equation 2 to determine the in-plane ionic conductivity (σ).

$$\sigma = \frac{L}{R \times t \times w} \qquad <2>$$

where σ was the in-plane conductivity, R was the in-plane membrane resistance, t was the membrane thickness (fully hydrated membrane) and w was the membrane width (fully hydrated membrane).

The through-plane ionic conductivity of SPEEK CEMs was determined using a concentration cell with 6 g L^{-1} of NaCl solutions in each compartment (the lower concentration value expected in the MDC). The solutions were agitated with magnetic stir bars. The active area for the cell was 2 cm^2. Each cell contained a platinum mesh working electrode (**Figure 5.c**). The resistance between the two working electrodes was measured with and without membranes using EIS in galvanostat mode (0.5 mA amplitude in the frequency range of 100,000 Hz to 0.1 Hz). The resistance was determined from the Bode plot, where the resistance value had a phase angle value of zero. The through-plane membrane resistance (R_m) was determined by subtracting the measured solution-membrane resistance ($R_{m\text{-}s}$) in the concentration cell minus the resistance of the supporting electrolyte (R_s - i.e., no membrane in the cell) [45] – see equation 3.

$$R_m[\Omega - cm^2] = (R_{m-s} - R_s) \cdot ActiveArea \qquad <3>$$

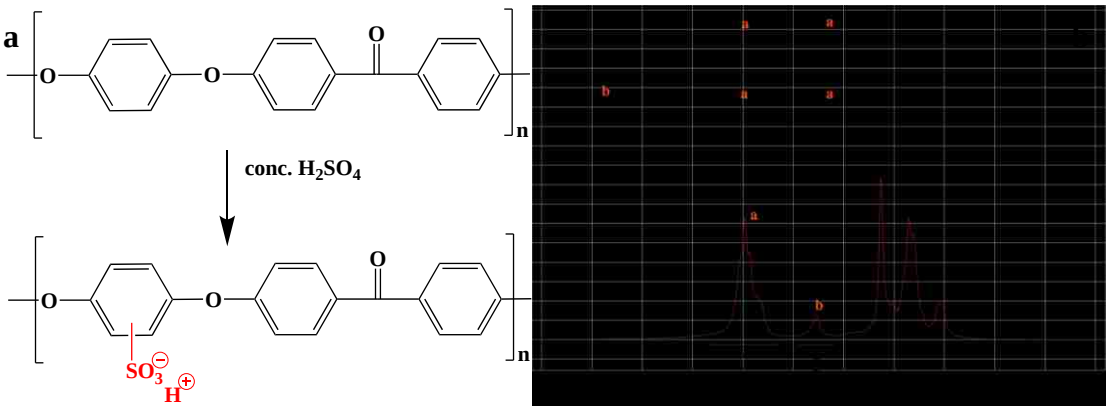

Figure 4. Synthesis scheme to make SPEEK (a) and ^{1}H NMR spectrum of prepared SPEEK (b).

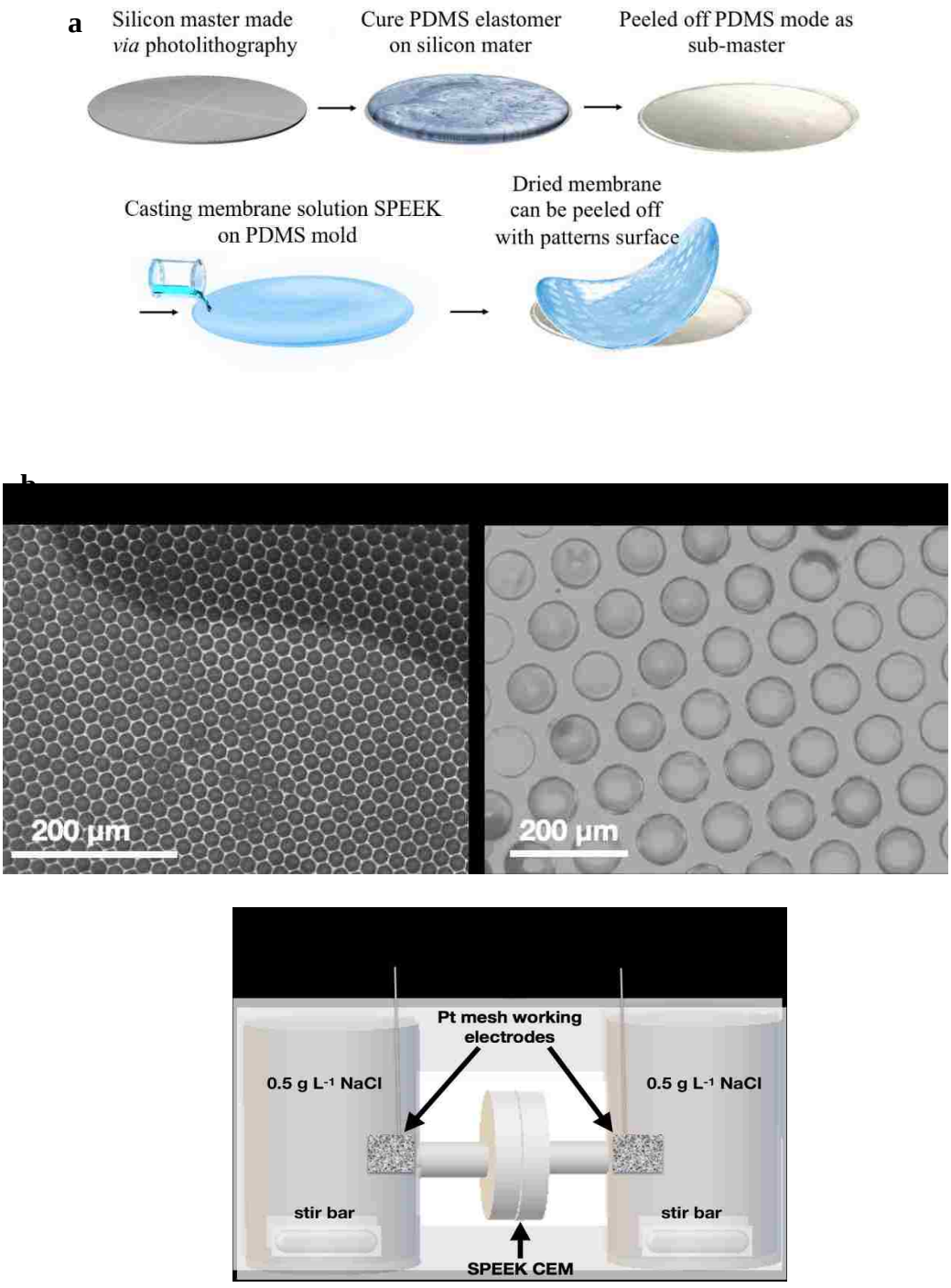

Figure 5. a.) Process flow to make micropatterned PDMS molds that are used for preparing topographically patterned SPEEK CEMs; b.) Optical micrograph images of SPEEK CEM S2 and S5 samples; c.) Concentration cell to measure the through-plane resistance and ionic conductivity for the SPEEK CEMs.

2.4. Measurements

2.4.1. Solution conductivity and pH

Solution conductivity and pH were measured, initially and 24 hours intervals during each cycle. An instrument Omega PHB- 600R (Omega Engineering Inc., Norwalk, CT, USA) was used to record pH. Solution conductivity was recorded using an instrument Orion Star 112 Conductivity Meter (ThermoFisher Scientific. Waltham, MA, USA). Both instruments were calibrated prior to the use.

2.4.2. Electrochemistry

Three days cycle (96 h) data was recorded by triplicate for each of the CEMs membranes and the commercial membrane, using the same setup and operating conditions, each cell was connected during the cycle to an external resistance of 470 Ω. Table 1 lists the membrane configurations tested in the MDC. At the end of each cycle (after 96 hr), the three chambers were filled with new electrolytes in order to have identical operating conditions for all the MDCs working with the different membranes and polarization curves were measured. In order to collect polarization curves to obtain the power curves, two potentiostats Gamry Reference 600+ (Gamry Instruments, PA, USA) were utilized and linear sweep voltammetries (LSVs) were run. The first potentiostat was operating from open circuit voltage (OCV) and 0 mV at a scan rate of 0.2 mV s-1. Particularly, the working channel was connected to the cathode, the counter channel was connected to the reference Ag/AgCl (3M KCl), with the reference channel was short circuited to the counter channel. In parallel, the second channel was recording the cathode potential during the LSV. Particularly, the working channel was connected to the cathode, the counter channel was connected to the anode and the reference channel was short circuited to the counter channel. Ag/AgCl (3M KCl) was used as

reference electrode and it was located into the desalination chamber. For both polarization and power curves, current and power are expressed as density values, referred to the cathode geometric area (7 cm^2) for cathode that is actually the same area as the AEM, and CEM.

Chapter 3. Results and Discussion

3.1. Patterned and non-patterned poly(2,6-dimethyl 1,4-phenylene) oxide based anion exchange membranes for enhanced desalination and power generation in a microbial desalination cell

3.1.1. Membranes characterization

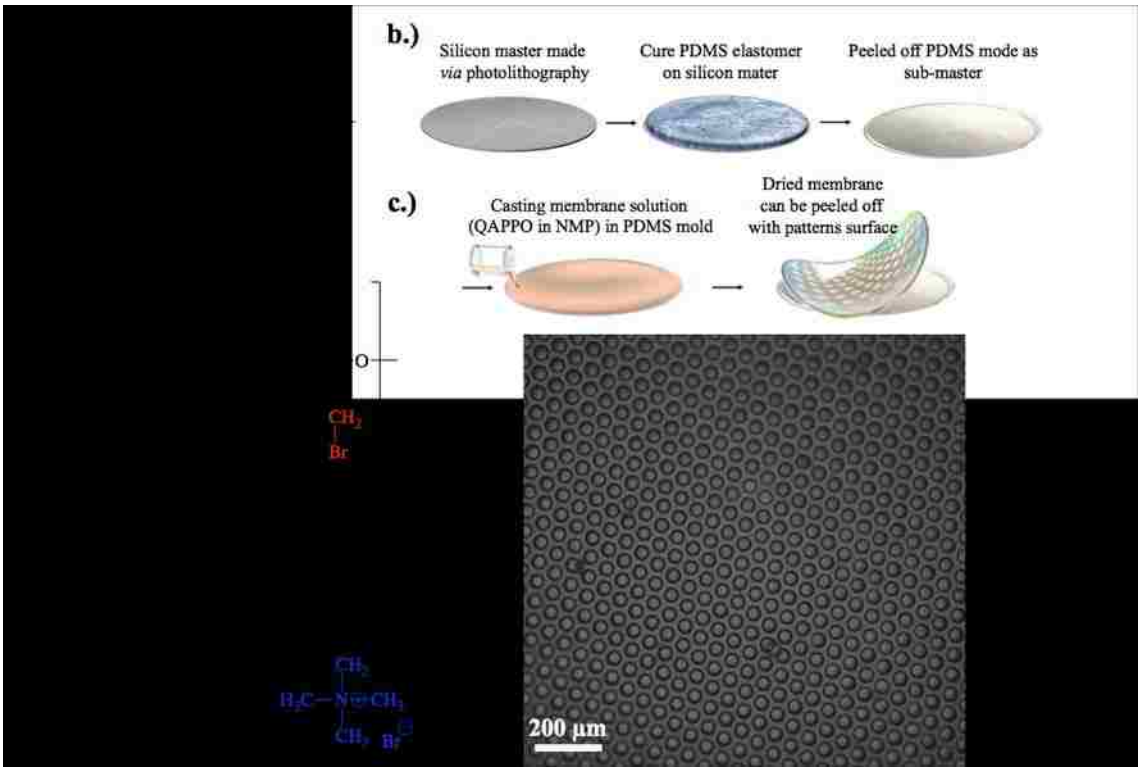

Figure 6. Scheme to synthesize of QAPPO AEMs (a); process flow scheme to make micropatterned QAPPO AEMs (b); and optical micrograph of QAPPO AEM with 40 µm lateral features (c).

Figure 6.a shows the scheme to synthesize QAPPO AEMs via free radical bromination of commercially available PPO. **Figure 6.b** is the process flow scheme to make reusable, micropatterned PDMS molds for fabricating QAPPO AEMs with

micropatterned well surfaces. **Figure 6.c** is an optical micrograph of a QAPPO AEM with 40 μm lateral features periodically spaced across the membrane surface.

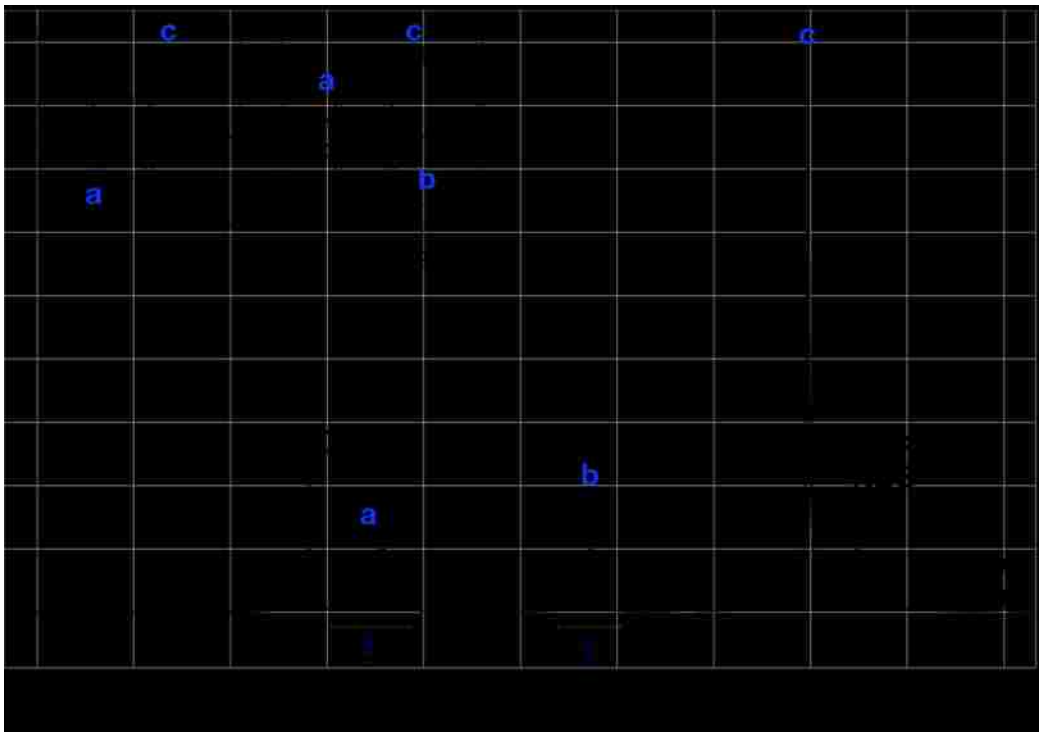

Figure 7: ^{1}H NMR spectrum of BrPPO.

Figure 7 is the ^{1}H NMR spectra of BrPPO. The signal at 4.5 ppm corresponds to the methylene moiety in the bromomethyl groups. The degree of functionalization (DF) value of the BrPPO is 0.51 (the fraction of repeat units with bromomehyl groups). The anion exchange groups, quaternary benzyl trimethylammonium groups, in PPO are formed by nucleophilic substitution of trimethylamine with the bromine moiety in the bromomethyl groups. For this study, QAPPO AEMs with a low ion-exchange capacity (IEC) (approx. 1.38 mmol g^{-1}) were prepared. The estimated IEC was calculated by the amount of trimethylamine added to the reaction with BrPPO and the DF value of BrPPO [46]. During the drop casting procedure, the unreacted bromomethyl groups self-crosslinked making the QAPPO AEMs insoluble for ^{1}H NMR analysis [42].

Table 1 reports the bulk, in-plane chloride ion conductivity of the non-patterned QAPPO AEMs. Because the chemistry of the patterned and non-patterned QAPPO AEMs is the same, no difference in ionic conductivity was expected.

Table 1: Chloride ion conductivity of QAPPO Q1 AEM in deionized water and saline solutions.

	σ in DI H_2O	σ in 5 ppm NaCl	σ in 50 ppm NaCl
QAPPO AEM in the chloride form	0.6 mS cm^{-1}	5.0 mS cm^{-1}	32.9 mS cm^{-1}

3.1.2. Power Curves

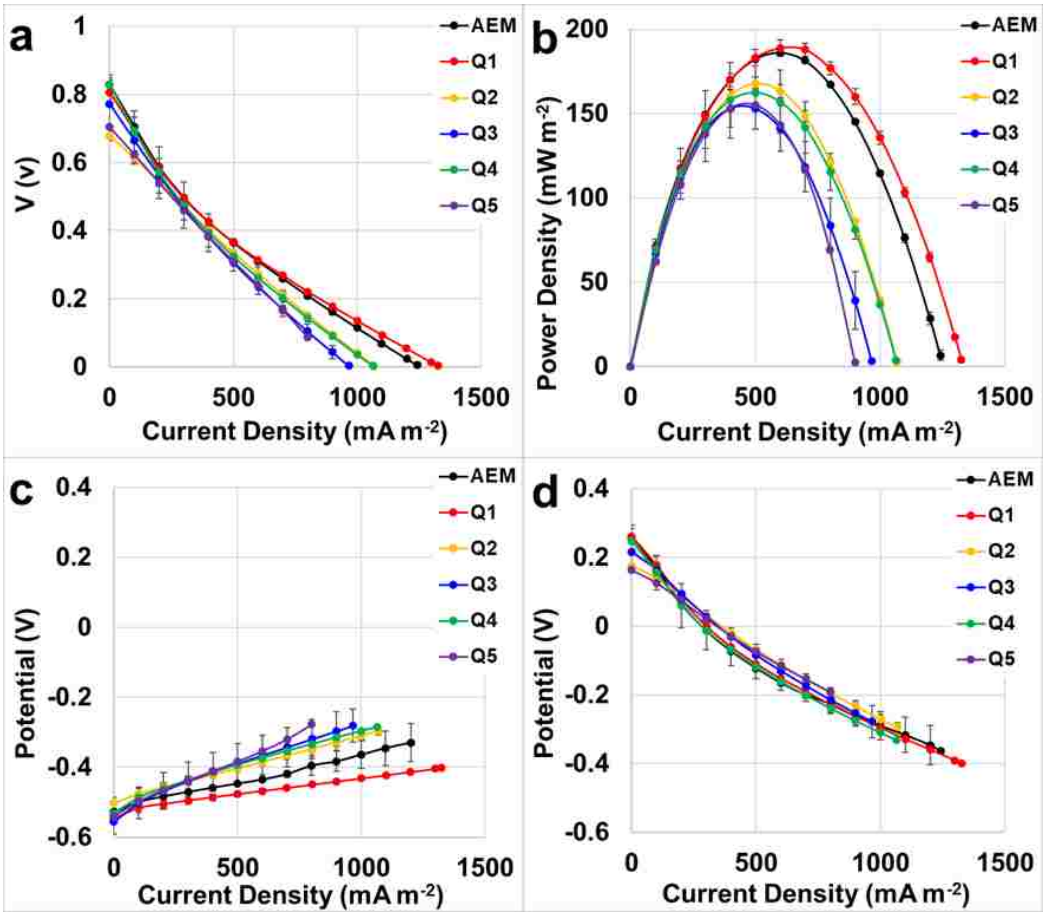

Figure 8. Overall polarization curve (a), power curves (b), anode (c) and cathode (d) polarization curves of the MDCs having different AEM.

Polarization curves (**Figure 8.a**), power curves (**Figure 8.b**), and anode (**Figure 8.c**) and cathode (**Figure 8.d**) polarization curves were obtained for the MDCs having different AEMs. In the graphs AEM corresponded to commercial AEM, and the Qs corresponded with the increase pattern surfaces 20(Q2), 33 (Q3), 40 (Q4), and 80 µm (Q5), following the same nomenclature in the rest of graphs. The only variable for these experiments was the type of AEM selected. As mentioned above, the electrochemical performance of the MDCs with different AEMs were acquired with initial fresh solutions, while the same and identical anode and cathode electrode were used.

The overall polarization curve (**Figure 8.a**) showed initial similar open circuit voltage (OCV) for all the membranes, with an average initial point of 0.75 ± 0.05 V, following similar trends for all the membranes investigated. Although, they had similar voltages at low current, higher voltages for AEM and Q1 were acquired at high current. Near to the short circuit, instead of the straight trend for Q2, Q3, Q4, and Q5; Q1 and the commercial membrane showed a slight different shape recording the maximum current densities at short circuit with 1325 mA m^{-2} for Q1 and 1242 mA m^{-2} for the commercial membrane AEM. Polarization curves displayed a linear trend indicating that the cell was largely governed by ohmic overpotentials (**Figure 8.a**).

Power curves were then obtained from the polarization curve. MDC with Q1 membrane recorded the maximum power density of 189±5 mW m^{-2} at a current density of 600 mA m^{-2}. The commercial membrane obtained slightly lower power generation (186 ± 0.1 mW m^{-2}). MDC with membranes Q2, Q3, Q4 and Q5 lower maximum points of power density recorded. Particularly, the power obtained were 167±4, 153±11, 162±12 and 155±5 mW m^{-2} respectively. Therefore, MDC with Q1 outperformed the power obtained by the MDC with commercial membrane. The addition of

topographical patterns on one side of the membrane did not give any advantage, actually electrochemical performance were worse than the AEM commercials.

The anode (**Figure 8.c**) and cathode (**Figure 8.d**) polarization curves were taken by inserting a reference electrode within the central chamber that was separated from the anode through the AEM and from the cathode through a CEM. The analysis of the polarization behavior of each electrode agreed with the overall polarization of the cell and their corresponding power curves trends. The polarization behavior of the anode (**Figure 8.c**) displayed linear trends in all cases, but with different slopes. The smaller the slope value corresponded with a smaller resistance that was associated with the type of membrane utilized. The results demonstrated that Q1 had the best performances followed by the commercial membrane and by Q2, Q4, Q3 and Q5 respectively. As the anodes utilized were identical in geometrical size and biofilm maturation, the different behavior was solely attributed to the membrane. With respect to the cathode overpotential (**Figure 8.d**), the polarization was relatively similar as the same electrode and membrane were used. Examining the cathode and anode polarization behavior together with the overall cell polarization demonstrates that the AEM resistance had a significant impact on power density and cell efficiency.

3.1.3. Desalination

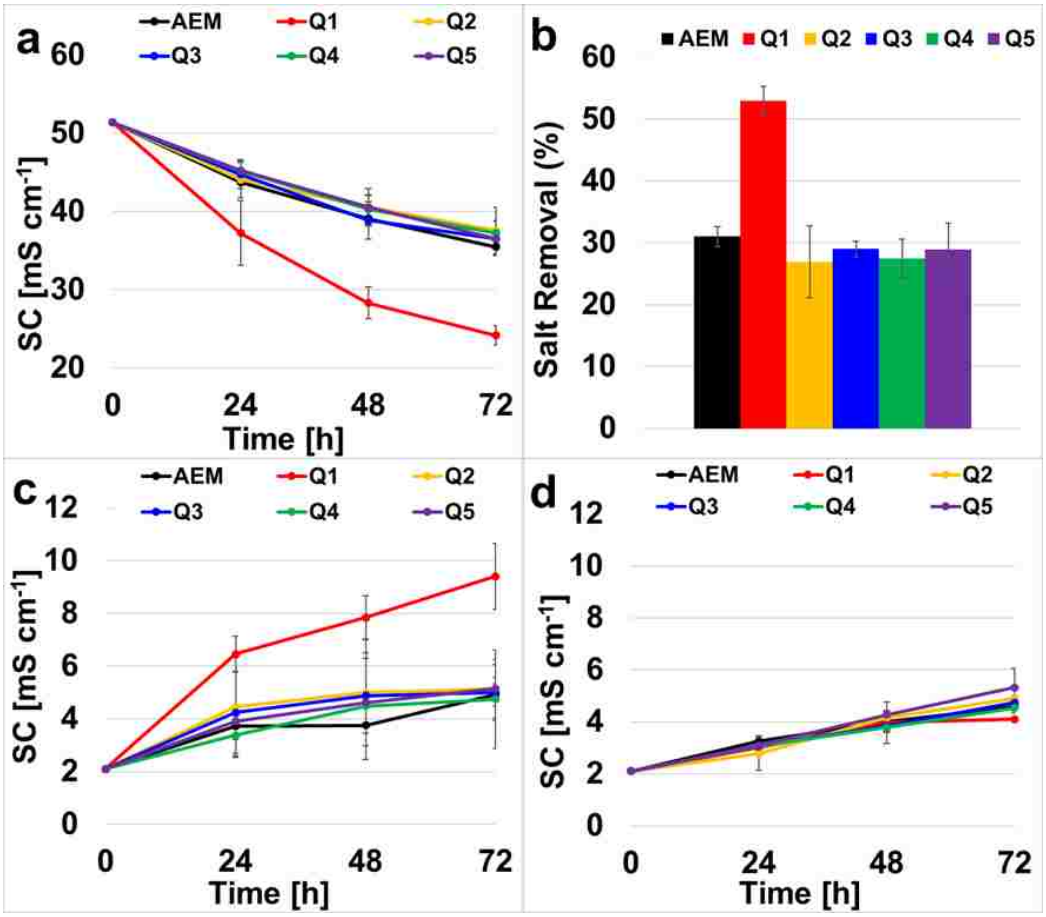

Figure 9. Desalination chamber solution conductivity (a), desalination chamber salt removal (b), anode chamber solution conductivity (c), cathode chamber solution conductivity (d).

The seawater conductivity and pH in the middle chamber of the MDC was 51.4 mS cm^{-1} and 7.8, respectively. Membrane Q1 provided the greatest removal of salt from the seawater (53±2.7%) and the solution conductivity at the end of the salt removal was 24.2±1.2 mS cm^{-1}. The patterned AEMs (Q2 to Q5) had roughly the same salt removal rate and drop in solution conductivity for the central chamber in the MDC (**Figures 9.a** and **Figure 9.b**). Hence, the micropatterned features did not seem to improve the desalination for the MDC. Furthermore, the non-patterned QAPPO AEM had the best performance signaling that the patterned membranes do not enhance desalination. One possible explanation for the lack of added benefit for the patterned membranes is that

they may be more prone to fouling. The motivation to use such patterned AEMs was to increase the interfacial area between the solution and the membrane to minimize interfacial resistance.

The solution conductivity of the anode and cathode chamber is given in **Figure 9.c** and **Figure 9.d**. The solution conductivity for both the anode and cathode increased because of the salt removal from the middle, desalination chamber through the ion-exchange membranes. The initial solution conductivity of the anode chamber (**Figure 9.c**) was 2.1 mS cm^{-1} and the final ionic conductivity, for all AEMs besides Q1 (i.e., Q2, Q3, Q4, Q5 and the commercial AEM) was 5.1 mS cm^{-1}. The final solution conductivity of the anode chamber featuring Q1 was 9.4±1.3 mS cm^{-1}, which was higher than the other membranes and corresponded to the greater desalination of the middle chamber.

The cathode chamber ionic conductivity (**Figure 9.d**), showed an increase from an initial of 2.1 mS cm^{-1}, to a final value of 4.5±0.5 mS cm^{-1} for all MDC experiments. The similar values observed were ascribed to the limitation that the same cation exchange membrane was used in all MDC experiments

3.1.4. pH variation

The pH of the anode chamber (**Figure 10.a**) decreased from an initial value of 7.8, to a final range of 6.0 to 6.8 measured at the end of MDC operation. This was due to the oxidation of organics and the production of H^+ as part of the final products therefore the anodic chamber tends to acidify. Charge neutrality is maintained due to the transport of chloride ions from the middle desalination chamber to the anode. The initial pH in the anode containing activated sludge was always 7.8. The pH of the cathode chamber increased from 7.8 up to 10 in every MDCs (**Figure 10.b**). This shift

in pH was due to the oxygen reduction reaction (ORR). In fact, the ORR can follow two different patterns: i) acidic with consumption of H^+ and production of water; or ii) alkaline with production of OH^-. It is not clear yet which ORR pattern is followed in neutral media but if the acidic way is preferred, H^+ is consumed from the solution and therefore and abundance of OH^- is generated. On the contrary, if the alkaline pattern is followed, the final product is OH^-. Both ORR patterns can explain the alkalization of the cathode chamber over time.

In order to maintain charge neutrality, sodium ions move from the desalination chamber to the cathode chamber through the cation exchange membrane. The initial pH for cathode was 7.8 and it climbed to a value of 10 at the end of the MDC runs. With respect to the desalination chamber (**Figure 10.c**) the pH remained relatively the same or slightly decreased probably because no electrochemical reactions with production/consumption of H^+ and OH^- are occurring.

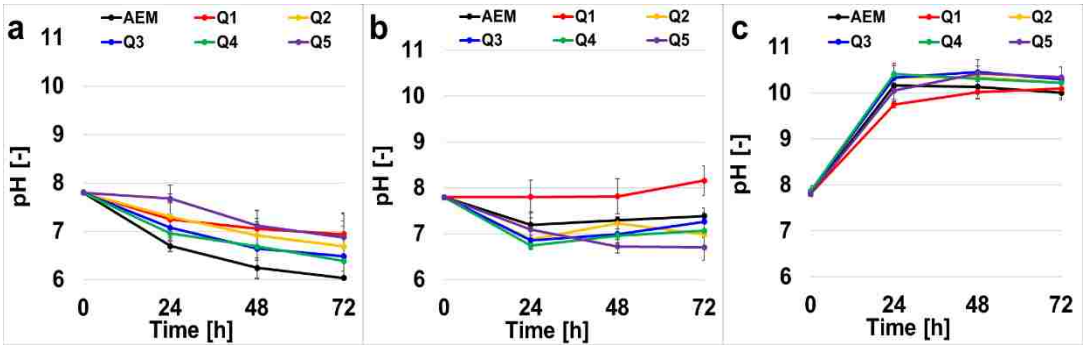

Figure 10. Anode chamber pH (a), desalination chamber pH (b) and cathode chamber pH (c).

3.2. Microbial desalination cell with sulfonated sodium polyether ether ketone as cation exchange membranes for enhancing power generation and desalination

3.2.1. Membranes characterization

Table 2. In-plane conductivity and through-plane resistance of SPEEK CEMs in different liquid solutions.

Sample	In-plane ionic conductivity (mS cm^{-1})			Through-plane resistance (Ω-cm^2)
	DI H_2O at 20 °C	DI H_2O at 40 °C	0.5 g L^{-1} NaCl at 20 °C	6 g L^{-1} NaCl at 20 °C
SPEEK CEM S1 - flat	2.9	10.7	320	23
SPEEK CEM S2 - 20 μm	n/a	6.5	291	38
SPEEK CEM S3 - 33 μm	n/a	8.2	288	28
SPEEK CEM S4 - 40 μm	n/a	6.6	290	23
SPEEK CEM S5 - 80 μm	3.7	5.6	333	24
Membranes International CMI-7000 CEM [47]	n/a	n/a	n/a	30*
n/a : non-applicable				*Note: 30g L^{-1} NaCl

Note: *Data from the supplier [47]. All CEMs' counterions are the sodium ion. The measured resistance for the 0.5 g L^{-1} NaCl solution for the concentration cell (for through-plane resistance measurements) was 1061 Ω-cm^2. The in-plane resistance for 0.5 g L^{-1} NaCl (with no membrane) was 262 Ω (9.5 mS cm^{-1}). The supporting electrolyte conductivity was selected from the in-plane conductivity of SPEEK CEMs in 0.5 g L^{-1} NaCl. n/a – the in-plane impedance, which is used to calculate the ionic conductivity, of the SPEEK CEMs was quite large under deionized water in the sodium counterion form at 20 °C. Therefore, testing whether or not the topographical patterns impacted ionic conductivity of the CEM was tested at elevated temperatures to reduce

the impedance and it was also tested with supporting electrolyte (0.5 g L^{-1}) because it also reduced the impedance. Plus, testing the membrane resistance/ionic conductivity of the SPEEK CEMs in supporting electrolyte rather than deionized water is more representative of the conditions in the MDC.

The ^{1}H NMR in **Figure 4.b** confirmed successful incorporation of sulfonic acid moieties into the PEEK polymer to make SPEEK, because a peak was detected at 7.5 ppm. The degree of sulfonation was 0.6 (i.e., the number of sulfonate groups per repeat unit) and that translated to an ion-exchange capacity (IEC) of 1.8 mmol g^{-1}. The 10 g batch of SPEEK synthesized was used to make all patterned and non-patterned SPEEK CEMs. The optical micrograph images in **Figure 5.b** verify the successful fabrication of periodic, topographical patterned features on the SPEEK CEMs. **Table 2** reports the in-plane ionic conductivity of the SPEEK CEMs in deionized water at different temperatures (20 °C and 40 °C) and in supporting electrolyte (0.5 g L^{-1} NaCl). Additionally, **Table 2** provides the through-plane resistance of the SPEEK CEMs. The in-plane ionic conductivity values showed high ionic conductivity values (296 to 342 mS cm^{-1}) in a dilute supporting electrolyte (0.5 g L^{-1}). This concentration of NaCl solution is substantially lower than the range of NaCl solutions in experienced in the MDC (6 to 30 g L^{-1}). There was no trend between micropatterned lateral feature size and SPEEK CEM ionic conductivity and through-plane resistance. It was hypothesized that patterning the CEM surface would increase the interfacial surface area between the membrane and the salt water in the desalination chamber. Having an increased interfacial area will enhance the rate of salt uptake, which should manifest a lower ohmic resistance and a higher cell power density and greater salt removal. However, the patterned membranes did not produce a MDC with greater power density or salt removal when compared to the flat (i.e., non-patterned) CEMs. It is important to point

out that the through-plane resistance and the in-plane resistance, characterized externally for the CEMs, was equivalent or worse with the patterned membranes. We ascribe the unexpected results to the following possibilities: i.) the patterned membranes trap small amount of particles or precipitates that hinder sodium ion transport and ii.) the micro-confined domains change the interface between the membrane and water slowing down the sodium ion migration. Similar results were observed for patterned and non-patterned AEMs in our previous study with MDC [48]. The impetus for using micropatterned ion-exchange membranes is from other reports showing that these materials enhance the performance of proton exchange membrane fuel cells with hydrogen [49]. However, that system is different than the MDC because the interface is a membrane-porous air cathode and here the interface is a membrane-water solution.

The flat SPEEK CEMs, in most cases, gave the highest in-plane ionic conductivity values and lowest through-plane resistance. It will be shown later that this membrane yielded the highest power output and desalination rate for the MDC indicating the patterned features did not provide any significant gains for the MDC – a same observation seen in our previous report for MDC with micropatterned AEMs [50].

Finally, it should be noted that all of the SPEEK CEMs had a lower through-plane resistance than the Membranes International CEM (data reported by the manufacturer) [47]. It should be noted that the Membranes International CEM was tested in a more concentrated supporting electrolyte when compared to our tests (approximately 30 g L^{-1} (0.5 M) NaCl). Because the SPEEK CEMs' resistance in 30 g L^{-1} NaCl was so low (on the order of 8 Ω-cm^2), the difference between the membrane-solution and solution resistance was almost zero - i.e., the membrane contribution to resistance could not be detected. The lower through-plane resistance and higher ionic

conductivity of the SPEEK CEMs, in addition to being thinner (50 μm versus 450 μm for the Membranes International CEM), indicated that these membranes were good candidates to lower the ohmic overpotential for the MDC.

Membrane ionic conductivity and thickness can be combined to calculate the area specific resistance (ASR) as shown below in equation R1. Note that the units for ASR are ohm-cm^2 (or cm^2 S^{-1}). In this equation, higher ionic conductivity yields a lower ASR. A thinner membrane also gives a smaller ASR. A membrane with both high ionic conductivity and a small thickness value work synergistically to drastically reduce the ASR. Reducing all the resistances within the MDC maximizes the power output and the desalination rate. A smaller ASR for both the AEM and CEM is critical for improving the thermodynamic efficiency and desalination performance of the MDC.

$$ASR = \frac{L}{\kappa} \qquad \text{<R1>}$$

L = membrane thickness

κ = membrane ionic conductivity

3.2.2. Power Curves

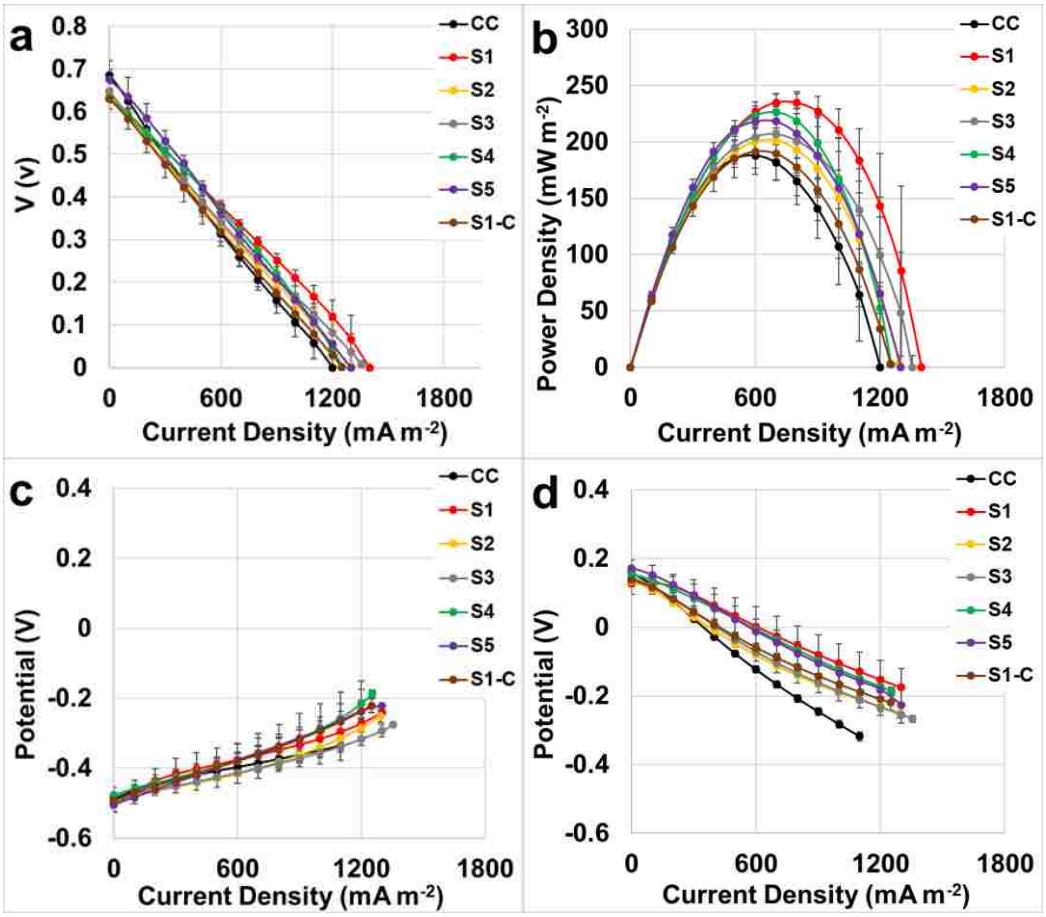

Figure 11. Overall polarization curve (a), power curves (b), anode (c) and cathode (d) polarization curves of the MDCs having different CEMs.

In the graphs CC corresponded to commercial AEM, S1 for non-pattern surface and the remain Ss corresponded with the increase pattern surfaces 20(S2), 33 (S3), 40 (S4), and 80 µm (S5). In case of S1C, is the combination of S1 with the commercial AEM already used for the former experiment .Following the same nomenclature in the rest of graphs.

MDCs were tested keeping the same AEM, in this case QAPPO 1, and changing the CEM among the previously described SPEEK membranes [48]. The electrochemical results are displayed in **Figure 11** and particularly, polarization curves (**Figure 11.a**), power curves (**Figure 11.b**), and anode (**Figure 11.c**) and cathode

(**Figure 11.d**) polarization curves were obtained. Polarization curves were recorded after anode and cathode solutions were replenished after the third day cycle in order to have identical operating conditions.

Initial open circuit voltage (OCV) of the MDCs showed as initial point (null current density) of the overall polarization curve (**Figure 11.a**) was similar for all the MDCs and quantified in 0.65±0.02 V. This value was independent from the membrane utilized. At short circuit current density, the utilization of commercial CEMs (CC) recorded the lowest value of 1200 mA m^{-2}. In parallel, a maximum short circuit current of 1399 mA m^{-2} was measured when S1 membrane was used as CEM. The short circuit average currents and the standard deviations (based on n = 3 measurements) obtained for each membrane were 1200±0.1 (CC), 1363±51.51 (S1), 1293±4.64 (S2), 1355±63.13 (S3), 1253±51.82 (S4), 1263±52(S5) and 1250±59.8 (S1-C) mA m^{-2}. The linear trends observed in the polarization curves highlight that MDC power output is governed by ohmic losses for all cases. These results suggest that future efforts should be geared towards minimizing ohmic overpotentials in MDC.

The power curves were calculated from polarization data according to the following equation: $P = I \times V$ (**Figure 11.b**). MDCs with membrane S1 (non-patterned) recorded the highest power density 235±7 mW m^{-2} at a current density of ≈700 mA m^{-2}. This result is ≈20% better than the best outcomes obtained in previous MDC study in which QAPPO was used as anion exchange membrane and commercial CEM [50]. Combination of both commercial anion and cation exchange membrane reached 188±11 mW m^{-2} at a current density of 600 mA m^{-2}, which was 20% lower in respects to S1 in terms of power generation. The MDCs having different membranes had a peak of power density of 201±19 mW m^{-2}, 204±16 mW m^{-2}, 226±16 mW m^{-2} and 218±13

mW m^{-2} for S2, S3, S4, and S5 respectively. These results are very similar and all below the S1 outcome. As observed in our previous study [50], the topographical patterns with different lateral sizes did not generate enhance power generation.

The anode (**Figure 11.c**) and cathode (**Figure 11.d**) polarization curves were obtained inserting the reference electrode in the central chamber and recording the potential variation during the polarization curve. The analysis of the anodic data sets shows similar trends for all the membranes, which was expected because the same identical membrane and the high-performing anode electrode was used. Negligible differences in potential (max of 40 mV) were detected at 600-700 mA m^{-2} in which the maximum power generations were recorded; therefore, the differences in power curves was attributed to the cathode. Considering the cathode polarization curves (**Figure 11.d**), different slopes in the trends were noticed for every different membrane utilized. The slope of the curve was ascribed to the ohmic losses, because identical cathodes materials and the same solution was used during the overall polarization curves. Hence, the higher resistance was related to the different membranes studied. The polarization curves revealed that S1 had the lowest ohmic resistance, while the CC had the highest ohmic resistance. These results demonstrate that reducing the membrane resistance lowered MDC polarization leading to greater power output.

3.2.3. Desalination

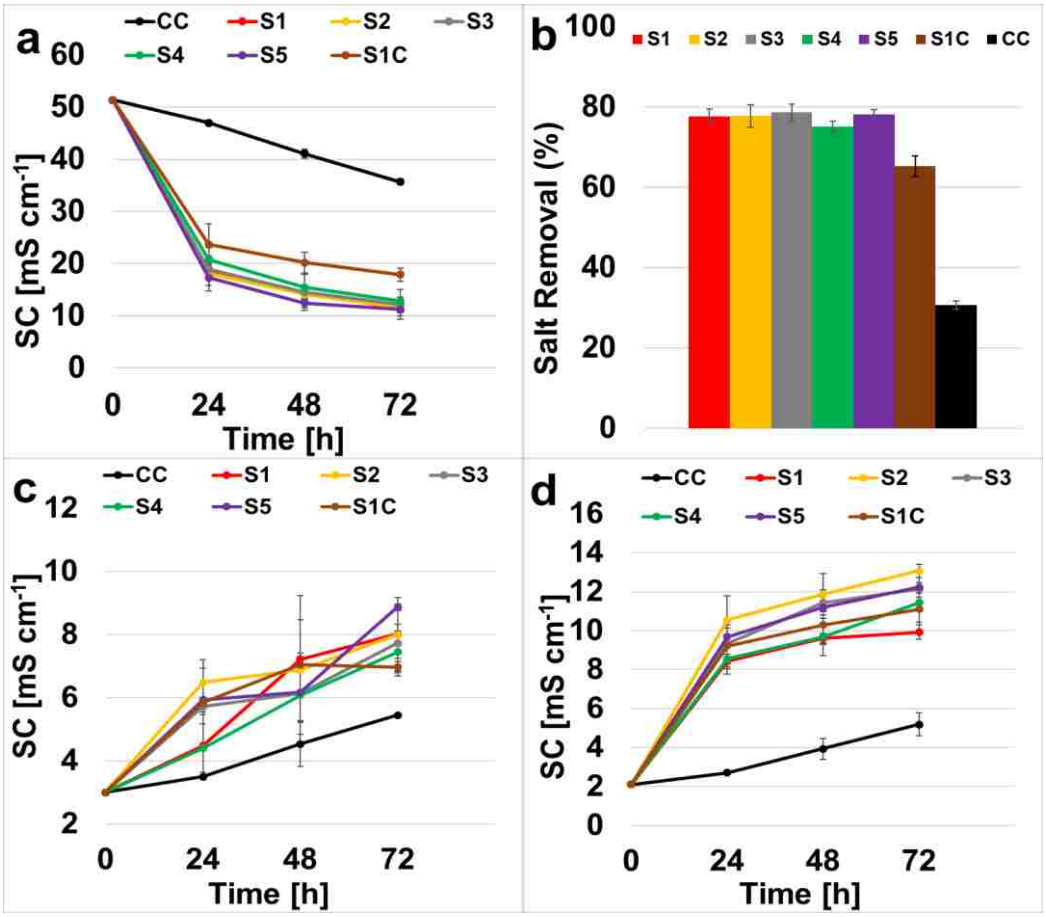

Figure 12. Desalination chamber solution conductivity (a), desalination chamber salt removal (b), anode chamber solution conductivity (c), cathode chamber solution conductivity (d).

The initial solution conductivity for the seawater placed in the desalination chamber at the start of each experiment was 51.4 mS cm^{-1}. The results displayed a final solution conductivity that was very similar and corresponded to 11.4±0.9 mS cm^{-1}, 11.4±1.4 mS cm^{-1}, 11±1 mS cm^{-1}, 12.8±0.7 mS cm^{-1}, 11.2±0.5 mS cm^{-1} for the utilization of membrane S1, S2, S3, S4 and S5 respectively (**Figure 12.a**). This corresponded to a reduction in salinity content of 77.7±1.8%, 77.7±2.7%, 78.6±2%, 75±1.4% and 78.2±1.1% respectively (**Figure 12.b**). Results did not show relevant differences between patterned and non-patterned membranes indicating that the lateral sizes did not play a major rule into the desalination. These amounts are much higher

than the recorded values by the combination of commercial membranes, which arrived up to 30.6±1% in terms of removal salt, with a final 35.7±0.5 mS cm^{-1}. These results gave a 25% improvement in terms of salt removal respect to the results obtained in the previous study using combination of commercial CEM and QAPPO AEM [50].

The solution conductivity at the anode chamber (**Figure 12.c**), that had an initial point of 2.1 mS cm^{-1}, showed a more variable picture with values that ranged between 7 mS cm^{-1} and 9 mS cm^{-1}. The trend was always increasing indicating a transport of negative ions from the desalination chamber to the anodic chamber. The cathode chamber was filled with the same buffer solution with initial solution conductivity of 2.1 mS cm^{-1} as start point. The increasing trend in solution conductivity was very similar for all the SPEEKs membranes reaching a maximum range between 10 mS cm^{-1} and 13 mS cm^{-1} that was 5 to 6-fold the initial value (**Figure 12.d**). A smaller increase, up to 4.6 mS cm^{-1}, was measured for the commercial membrane, because this membrane transferred fewer ions.

3.2.4. pH variation

The pH was another important parameter that was monitored over time. Activated sludge taken from the same existing batch was used in each cell for anode chamber, with an initial pH of 7.8 (**Figure 13.a**). This initial value decreased up to 6.8±0.2 for all SPEEKs membranes, and up to a lower value of 7.1±0.1 for the commercial membrane. This decrease might be explained by the increase of H^+ concentration as a product of the oxidation of organics, leading to an acidification of the media. In the case of cathode chamber (**Figure 13.b**), the initial buffer pH was also 7.8, but inversely here, the values displayed incremented up to 9.81±0.15. This value was very similar for all the cells independently from the membrane utilized.

This can be attributed to the products of the oxygen reduction reaction (ORR) produced at the cathode. In fact, the reaction at the cathode can proceed two different directions in function of the working electrolyte (e.g. acidic or alkaline). As the reaction occurs in acidic media, H^+ is consumed and water is produced. In parallel, if the reaction takes place in alkaline media, OH^- is the final product. Both ORR pathways lead to the alkalization of the cathode chamber over time and this can be attributed to i) the consumption of H^+ or ii) to the production of OH^-.

The desalination chamber (**Figure 13.c**) that was filled with the seawater had an initial pH value of 7.8, showed a more stable trend ending in a range between 7.4 and 8. This stability was probably due to the absence of electrochemical reactions occurring in this specific chamber.

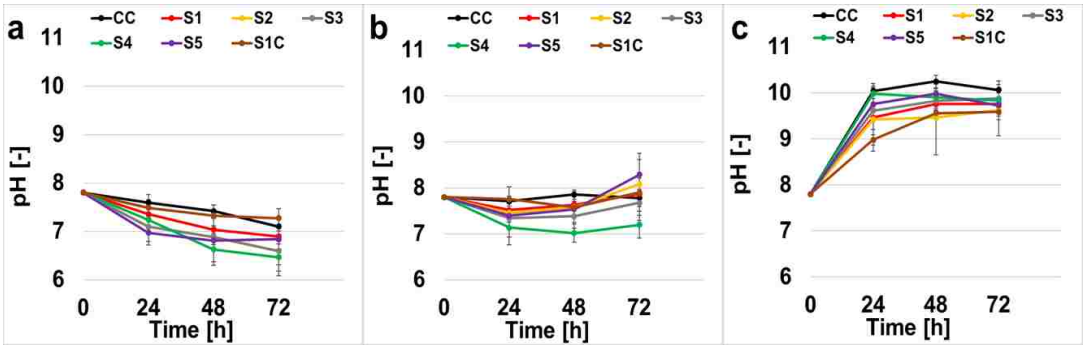

Figure 13. Anode chamber pH (a), desalination chamber pH (b), cathode chamber pH (c).

3.2.5. CEM long term performance and cost

The CEMs are anticipated to be stable for the long-term as the sodium chloride solution in the desalination chamber is benign. The CEM does interface with the air cathode and oxygen reduction can yield reactive oxygen species (ROS). The polyaromatic nature of the SPEEK backbone will make it resistant to oxidation by ROS. The ROS expected in the catholyte will be superoxide as this species is favored under alkaline conditions [50-51]. Strong oxidizing agents like hydroxyl and hydroperoxyl radicals, formed from the decomposition of hydrogen peroxide (parasitic product from oxygen reduction), are favored under acidic conditions [52-53]. The steady-state pH of the catholyte chamber of the MDC is 9.5 to 10 supporting a basic environment in the catholyte chamber. Therefore, the polyaromatic nature of the SPEEK and absence of hydroxyl and hydroperoxyl radicals suggest that the CEM will be stable for extended periods of time. Future efforts will need to examine SPEEK stability in the presence of superoxide species.

The laboratory membrane costs are quite low compared to membranes sold on the market. These are prepared from low cost and abundant commercially available poly(arylene ether) polymers using simple and straightforward reactions. Recently the price of these membranes is estimated at \$198 per m^2, but through scale-up, the membranes based upon the poly(arylene ether) polymers could be priced as low as \$2 per m^2 [54]. Electrodialysis membranes by Tokuyama (industry leader), quoted from Ameridia (a supplier for Tokuyama), are \$356 per m^2 on public prices. However, we do not know fabrication prices so that we cannot confirm relevant differences.

Chapter 4: Conclusions

Utilizing thinner and more conductive AEMs and CEMs, prepared by functionalizing commercially available polymers with ionic groups using facile and established procedures, enhanced the power output and desalination rate for MDC when compared to baseline studies that employed thick AEMs and CEMs that have low ionic conductivity. Laboratory made AEM and CEM combined in this specific MDC obtained the maximum power generation during this investigation of 235±7 mW m^{-2} at 700 mA m^{-2}, which is approximately 20% better than commercial membranes tested. Solution conductivity decreased by 60% within the first 24 hours and up to 80% after 3 days substantiating the desalination process, instead of 31% for commercial membranes. The pH increased above 9.5 after 24 hours due to the alkalization of the cathode. Membranes with non-patterned surfaces outperformed membranes with different topographic patterns of varying lateral feature sizes. The ionic conductivity of the flat membranes was slightly higher than the patterned membranes and is the reason why the flat membranes yielded the best power output and desalination rate. Hence, the added processing of patterning membranes to increase greater interfacial area between the liquid solution and the membrane to reduce interfacial charge-transfer resistance did not occur as hypothesized.

The results in terms of power generation are still lower than the ones existing in literature [33]. However, in terms of desalination, the results are much closer to the existing reported values and in many cases, even better than the results obtained in other studies with similar MDC systems, taking account the utilization of synthetic salt waters with initial solution conductivity values of 30-35 mS cm^{-1} [13,14,55,56]. The reduction of dissolved salt in the desalination chamber over time causes an increased resistance from this chamber over time. This is often seen in electrodialysis and reverse

electrodialysis in which the dilute chamber is the biggest source of resistance [57]. One strategy to combat this problem is to load a porous bed into the desalination chamber that conducts ions but does not add ions to the liquid phase, using a similar approach to that for electro deionization [58]. However, a porous resin-wafer [59] is more effective than a packed column that is commonly used in electrode ionization. Lower performances compared to existing literature can be attributed to the limitations in the current experiments due to the low operating temperature (room temperature of 22±2 °C) as low temperatures hinder the anode oxidation reactions kinetics, as well as the activated sludge used in this investigation had a very low solution conductivity (2.1 mS cm^{-1}) that negatively affects the performances.

Chapter 5. Outlook

The principal limitation for real application of MDC systems is the difficulty to scale up, there are issues to address as inefficient rates of power generation for larger scales, thick biofilm formation at anode reduces efficiency due to decrease in anodic activity, very thin membranes with better properties that could implicate more difficulty to assemble and liquid leakages, and lack of efficient recirculation system. From our results, we are encouraged to continue efforts to improve the membranes for MDC. Lowering the resistance will still be a priority in addition to enhancing the chemical and physical stability so they can operate effective for long time use and many cycles. Testing these membranes with flow recirculation in order to assess life-cycle and reuse. Also, it would be interesting developing selective membranes for remediation of specific compounds or contaminants.

Chapter 6. Acknowledgements

Funding for this research was provided by National Science Foundation Award CAREER #1652619 and EPSCoR #IIA-1301346. National Science Foundation Award #1703307. Also, Bill & Melinda Gates Foundation grant: ‘‘Efficient Microbial Bio-electrochemical Systems” (OPP1139954).

Author(s) also thank LSU’s Center for Advanced Microstructures (CAMD) for access to the optical microscope, the Chemistry Department at LSU for use of the 400 MHz Bruker NMR spectrometer, and Ms. Le Zhang for preparing the process flow diagram that depicts fabrication for patterned QAPPO AEMs and SPEEK CEMs

Any opinions, findings, and conclusions or recommendations expressed in this publication are those of the author(s) and do not necessarily reflect the views of the National Science Foundation.

References

[1] M. Falkenmark, C. Widstrand. Population and water resources: a delicate balance. Popul. Bull. 47, 1992, 1-36.

[2] T. Oki, S. Kanae. Global hydrological cycles and world water resources. Science 313, 2006, 1068-1072

[3] I.A. Shiklomanov. Appraisal and Assessment of World Water. Water Int. 25, 2000, 11-32

[4] M. Nair, D. Kumar. Water desalination and challenges: The Middle East perspective: a review. Desalination Water Treat. 51, 2013, 2030-2040.

[5] I.C. Karagiannis, P.G. Soldatos PG. Water desalination cost literature: review and assessment. Desalination 223, 2008, 448-456.

[6] M.K. Wittholz, B.K. O'Neill, C.B. Colby, D. Lewis. Estimating the cost of desalination plants using a cost database. Desalination 229, 2008, 10-20.

[7] A. Al-Karaghouli, L.L. Kazmerski. Energy consumption and water production cost of conventional and renewable-energy-powered desalination processes. Renew. Sustainable Energy Rev. 24, 2013, 343–356

[8] L.F. Greenlee, D.F. Lawler, B.D. Freeman, B. Marrot, P. Moulin. Reverse osmosis desalination: water sources, technology, and today's challenges. Water Res. 43, 2009, 2317-2348.

[9] A. Pérez-González, A.M. Urtiaga, R. Ibáñez, I. Ortiz. State of the art and review on the treatment technologies of water reverse osmosis concentrates. Water Res. 46, 2012, 267-283.

[10] M. Gryta. Long-term performance of membrane distillation process. J. Membr. Sci. 265, 2005, 153–159.

[11] E. Curcio, E. Drioli. Membrane Distillation and Related Operations—A Review. Sep. Purif. Rev. 34, 2005, 35-86.

[12] K. Peng Lee, T.C. Arnot, D. Mattia. A review of reverse osmosis membrane materials for desalination-development to date and future potential. J. Membr. Sci. 370, 2011, 1–22

[13] S. Lee, C. Boo, M. Elimelech, S. Hong. Comparison of fouling behavior in forward osmosis (FO) and reverse osmosis (RO). J. Membr. Sci. 365, 2010, 34–39

[14] X. Cao, X. Huang, P. Liang, K. Xiao, Y. Zhou, X. Zhang, B.E. Logan. A new method for water desalination using microbial desalination cells. Environ. Sci. Technol. 43, 2009, 7148-7152.

[15] H.M. Saeed, G.A. Husseini, S. Yousef, J. Saif, S. Al-Asheh, A. Fara, S. Azzam, R. Khawaga, A. Aidan. Microbial desalination cell technology: a review and a case study. Desalination 359, 2015, 1-13.

[16] A. Carmalin Sophia, V.M. Bhalambaal, E.C. Lima, M. Thirunavoukkarasu. Microbial desalination cell technology: Contribution to sustainable waste water treatment process, current status and future applications. J. Environmental Chemical Engineering 4, 2016, 3468–3478

[17] H. Wang, Z.J. Ren. A comprehensive review of microbial electrochemical systems as a platform technology. Biotechnol. Adv. 31, 2013, 1796-1807.

[18] C. Santoro, C. Arbizzani, B. Erable, I. Ieropoulos. Microbial Fuel Cells: from Fundamentals to Applications. A review. J. Power Sources 356, 2017, 225-244.

[19] A. Dekker, A. T. Heijne, M. Saakes, H. V. Hamelers, C. J. Buisman, Analysis and improvement of a scaled-up and stacked microbial fuel cell. Environmental science & technology, 43(23), 2009, 9038-9042.

[20] D. Jiang, M. Curtis, E. Troop, K. Scheible, J. McGrath, B. Hu, B. Li, A pilot-scale study on utilizing multi-anode/cathode microbial fuel cells (MAC MFCs) to enhance the power production in wastewater treatment. international journal of hydrogen energy, 36(1), 2011, 876-884.

[21] H. Hiegemann, D. Herzer, E. Nettmann, M. Lübken, P. Schulte, K. G. Schmelz, M. Wichern, An integrated 45L pilot microbial fuel cell system at a full-scale wastewater treatment plant. Bioresource technology, 218, 2016, 115-122.

[22] S. Wu, H. Li, X. Zhou, P. Liang, X. Zhang, Y. Jiang, X. Huang, A novel pilot-scale stacked microbial fuel cell for efficient electricity generation and wastewater treatment. Water research, 98, 2016, 396-403.

[23] Y. Feng, W. He, J. Liu, X. Wang, Y. Qu, N. Ren, A horizontal plug flow and stackable pilot microbial fuel cell for municipal wastewater treatment. Bioresource technology, 156, 2014, 132-138.

[24] R. D. Cusick, B. Bryan, D. S. Parker, M. D. Merrill, M. Mehanna, P. D. Kiely, B. E. Logan, Performance of a pilot-scale continuous flow microbial electrolysis cell fed winery wastewater. Applied microbiology and biotechnology, 89(6), 2011, 2053-2063.

[25] F. Zhang, Z. He, Scaling up microbial desalination cell system with a post-aerobic process for simultaneous wastewater treatment and seawater desalination. Desalination 360, 2015, 28-34.

[26] Q. Ping, B. Cohen, C. Dosoretz, Z. He. Long-term investigation of fouling of cation and anion exchange membranes in microbial desalination cells. Desalination 325, 2013, 48-55

[27] K.S. Brastad, Z. He. Water softening using microbial desalination cell technology. Desalination 309, 2013, 32-37.

[28] S. Sevda, H. Yuan, Z. He, I.M. Abu-Reesh. Microbial desalination cells as a versatile technology: Functions, optimization and prospective. Desalination 371, 2015, 9-17

[29] K.S. Jacobson, D.M. Drew, Z. He. Efficient salt removal in a continuously operated upflow microbial desalination cell with an air cathode. Bioresour. Technol. 102 (1), 2011, 376-380

[30] Z. Borjas, A. Esteve-Núñez, J.M. Ortiz. Strategies for merging microbial fuel cell technologies in water desalination processes: Start-up protocol and desalination efficiency assessment. J. Power Sources 356, 2017, 519-528.

[31] H. Luo, P. Xu, T.M. Roane, P.E. Jenkins, J. Ren. Microbial desalination cells for improved performance in wastewater treatment, electricity production, and desalination. Bioresour. Technol. 105, 2012, 60–66.

[32] Y. Li, J. Styczynski, Y. Huang, Z. Xu, J. McCutcheon, B. Li. Energy-positive wastewater treatment and desalination in an integrated microbial desalination cell (MDC)-microbial electrolysis cell (MEC). J. Power Sources 356, 2017, 529-538.

[33] Y. Qu, Y. Feng, X. Wang, J. Liu, J. Lv, W. He, B.E. Logan. Simultaneous water desalination and electricity generation in a microbial desalination cell with electrolyte recirculation for pH control. Bioresour. Technol. 106, 2012, 89–94.

[34] D. Ucar, Y. Zhang, I. Angelidaki. An Overview of Electron Acceptors in Microbial Fuel Cells. Front. Microbiol. 8, 2017, 643

[35] Y. Kim, B.E. Logan. Microbial desalination cells for energy production and desalination. Desalination 308, 2013, 122–130

[36] F. Soavi, L.G. Bettini, P Piseri, P Milani, C Santoro, P. Atanassov, C. Arbizzani, Miniaturized supercapacitors: key materials and structures towards autonomous and sustainable devices and systems, J. Power Sources 326, 2016, 717-725.

[37] M. Kodali, R. Gokhale, C. Santoro, A. Serov, K. Artyushkova, P. Atanassov, High Performance Platinum Group Metal-free cathode Catalysts for Microbial Fuel Cell (MFC), J. Electrochem. Soc. 164, 2017, H3041-H3046.

[38] C. Santoro, F. Benito Abad, A. Serov, M. Kodali, K.J. Howe, F. Soavi, P. Atanassov. Supercapacitive Microbial Desalination Cells: New Class of Power Generating Devices for Reduction of Salinity Content. Appl. Energy 208, 2017, 25-36.

[39] C. Santoro, M. Rezeai Talarposhti, M. Kodali, R. Gokhale, A. Serov, I. Merino-Jimenez, I. Ieropoulos, P. Atanassov. Microbial desalination cells with efficient platinum group metal-free cathode catalysts. ChemElectroChem, doi: 10.1002/celc.201700626

[40] C. Arges, L. Wang, J. Parrondo, V. Ramani. Best Practices for Investigating Anion Exchange Membrane Suitability for Alkaline Electrochemical Devices: Case Study Using Quaternary Ammonium Poly(2,6-dimethyl 1,4-phenylene)oxide Anion Exchange Membranes. J. Electrochem. Soc. 160, 2013, F1258-F1274.

[41] S. Gu, R. Cai, Y. Yan. Self-crosslinking for dimensionally stable and solvent-resistant quaternary phosphonium based hydroxide exchange membranes. Chem. Commun. 47, 2011, 2856-2858.

[42] AMI-7001S Anion Exchange Membranes Technical Specifications. https://www.membranesinternational.com/tech-ami.htm

[43] S. Sambandam and V. Ramani, Influence of binder properties on kinetic and transport processes in polymer electrolyte fuel cell electrodes, Phys.Chem. Chem.Phys. 12, 2010, 6140-6149.

[44] L. Zhang, T. Porter, S. Guillory, C. Cao and C. G. Arges, Patterning Polymer Electrolyte Membrane for Fuel Cell and Electrolysis Applications, ECS Trans. 77, 2017, 1325-1335.

[45] B. Bauer, H. Strathmann, F. Effenberger, Anion exchange membranes with improved alkaline stability, Desalination 79, 1990, 125-144.

[46] C.G. Arges, L. Wang, M.-s. Jung, V. Ramani. Mechanically stable poly (arylene ether) anion exchange membranes prepared from commercially available polymers for alkaline electrochemical devices. J. Electrochem. Soc. 162, 2015, F686-F693.

[47] CMI-7000S Cation Exchange Membranes Technical Specifications, in, Membranes International Inc.

[48] F. Lopez Moruno, J.E. Rubio, C. Santoro, P Atanassov, J.M. Cerrato, C.G. Arges, Investigation of patterned and non-patterned poly (2,6-dimethyl 1,4-phenylene) oxide based anion exchange membranes for enhanced desalination and power generation in a microbial desalination cell, Solid State Ionics. 341, 2018, 141-148.

[49] Y. Jeon, D. J. Kim, J. K. Koh, Y. Ji, J. H. Kim, Y. G. Shul, Interface-designed membranes with shape-controlled patterns for high-performance polymer electrolyte membrane fuel cells. Scientific reports, 5, 2015, 16394.

[50] J. Parrondo, Z. Wang, M.-S. J. Jung, V. Ramani, Reactive oxygen species accelerate degradation of anion exchange membranes based on polyphenylene oxide in alkaline environments. Physical Chemistry Chemical Physics 18, 2016, 19705-19712.

[51] Y. Zhang, J. Parrondo, S. Sankarasubramanian, V. Ramani, Detection of Reactive Oxygen Species in Anion Exchange Membrane Fuel Cells using In Situ Fluorescence Spectroscopy. ChemSusChem 10, 2017, 3056–3062.

[52] V. Prabhakaran, C. G. Arges, V. Ramani, Investigation of polymer electrolyte membrane chemical degradation and degradation mitigation using in situ

fluorescence spectroscopy. Proceedings of the National Academy of Sciences of the United States of America 109, 2012, 1029-1034.

[53] V. Prabhakaran, C. G. Arges, V. Ramani, In situ fluorescence spectroscopy correlates ionomer degradation to reactive oxygen species generation in an operating fuel cell. Phys Chem Phys 15, 2013, 18965-18972.

[54] S. Gu, R. Cai, T. Luo, K. Jensen, C. Contreras, Y. Yan, Quaternary phosphonium-based polymers as hydroxide exchange membranes. ChemSusChem, 3(5), 2010, 555-558.

[55] C. Forrestal, P. Xu, P.E. Jenkins, Z.J. Ren, Microbial desalination cell with capacitive adsorption for ion migration control, Bioresour., Technol, 120, 2012, 332-336.

[56] A. ElMekawy, H.M. Hegab, D. Pant, The near-future integration of microbial desalination cells with reverse osmosis technology, Energy Environ. Sci., 7, 2014, 3921-3933.

[57] H. Strathmann, A. Grabowski, G. Eigenberger, Ion-Exchange Membranes in the Chemical Process Industry. Industrial & Engineering Chemistry Research, 52, 2013, 10364-10379.

[58] J. Wood, J. Gifford, J. Arba, M. Shaw, Production of ultrapure water by continuous electrodeionization. Desalination 250, 2010, 973-976.

[59] S. Datta, M. P. Henry, Y. J. Lin, A. T. Fracaro, C. S. Millard, S. W. Snyder, ... & R. W. Dorner, Electrochemical CO2 capture using resin-wafer electrodeionization. Industrial & Engineering Chemistry Research, 52(43), 2013, 15177-15186.